Heat Transfer Enhancement of a Heating Flat using Turbulent Spots by Variation of Injected Velocity

Sudarat Srichan[1*], Wannarat Rakpakdee[2], and Weerachai Chaiworapuek[2]

1 Department of Mechanical Engineering, Faculty of Engineering, Rangsit University, Pathum Thani, Thailand
2 Department of Mechanical Engineering, Faculty of Engineering, Kasetsart University, Bangkok, Thailand
[*]Corresponding author, E-mail: sudarat.s@rsu.ac.th

Abstract

This paper studies Turbulent spots which is an effective technique that required very small input power to increase the rate of heat transfer on a flat plate. The effect of boundary layer destabilization by water injection on structural as well as thermal behaviors of a turbulent spot in a low turbulent water tunnel on a flat heating plate using the coating thermochromic liquid crystals were investigated. The local Reynolds number of the mainstream flow was controlled to be in the range between 61,000 to 130,000 at the experimental site. This experiment observed both single spot and longitudinal merging spots which were formed by the different duration of water injection 50.53 and 101.06 s. The experiment is divided into 2 cases with the differences of isothermal surface temperature, the temperature of the mainstream and injected velocity at 28 °C, 24 °C and 13 m/s and at 27 °C, 23 °C and 15 m/s, respectively. From the flow visualization technique using the liquid crystals and the image processing method, the thermal characteristics of the turbulent spot were obtained as the contours of Nusselt number and the turbulent spot effectiveness. When there was a difference in temperature (heat exchanger), the value of Nusselt number and effectiveness would be able to estimate. In the same different range of temperature, i.e. 4 °C, the different results of the single spot were not significant. Moreover, the results of heat transfer enhancement of the single spot and two spots via different injected velocity are compared and discussed. These obtained results are important information to develop the process of heat transfer augmentation over the flat plate flow.

Keywords: *Turbulent spot, Boundary layer, Transition, Longitudinal Merging Spots, Liquid crystals*

1. Introduction

Nowadays, heat transfer improvement techniques are commonly used in various engineering areas such as air-conditioning equipment, evaporators, process industries, thermal power plants, refrigeration systems; in order to decrease the operating cost by increasing the system efficiency. Three different techniques of heat transfer enhancement, including passive, active and compound techniques are normally used to gain thermal efficiency and overall efficiency. The passive technique does not need any external power input but to utilize rough surfaces, extended surfaces, displaced enhancement devices, swirl flow devices, or additives to improve the heat transfer. On the other hand, the active techniques involve some external power input for the enhancement of heat transfer such as mechanical aids, surface vibration, fluid vibration, injection, jet impingement. Lastly, the compound technique involves complex design but has limited applications. Nevertheless, it has been found that a turbulent spot, which is an active technique, has the potential to augment the heat transfer by artificially initiating on the flat plate under the laminar boundary layer. With a small input power for the spot generation, the turbulent spot can improve the heat transfer rate up to 15 % during Re_x = 61,000 – 130,000 (Sabatino, & Smith, 2008). Furthermore, the heat transfer rate is still increasing when the turbulent spot propagates further downstream.

1.1. Single turbulent spot and longitudinal merging spots

According to the turbulent level, the fluid flow can be classified using Reynolds number (*Re*) as laminar, transition, and turbulent flows. When the *Re* is more than the critical Reynolds number, the flow is considered as turbulent flow. Otherwise, it is laminar. The turbulent spot is an important phenomenon under boundary layer transition and found as a small turbulent patch, surrounding by laminar flow. Emmons et al., (1951), who first discovered the turbulent spot, suggested that the distribution of intermittency factor in the

Proceedings of RSU Research Conference (2019)

transition region could be described as a function of the parameters such as growth rate, convection velocity, and spot production rate. His model considered the turbulent region in a transitional boundary layer as the simple superposition of independently developed turbulent spots. Afterward, Elder (1960) and Sokolov et al. (1986) verified that two partially merging turbulent spots occupied almost the same turbulent area as the simple superposition of their outlines. From Emmons's assumption, showing that no interaction between spots. Schubauer and Klebanoff (1955) investigated the spot behavior experimentally using hotwire anemometer. They found that the spot features such as leading edge, trailing edge, becalmed region, for instance, can be illustrated as shown in Figure 1. The shape of the turbulent spot exhibited an arrowhead-like structure. The velocity of the leading and trailing edges are 88 % and 50 % of free stream velocity, respectively. In 1976, Wygnanski postulated that a spot grows in the streamwise direction by the continual addition of hairpin vortices at the spot trailing edge. With the advection and merging processes of the turbulent spots, these isolated hairpin forests develop into the downstream turbulent region (Wu, & Moin, 2010). Hence, the increase of heat transfer rate, occurring in the transition region is mainly caused by the turbulent spots. Particularly, the highest surface heat transfer occurs at the trailing or calmed region of a turbulent spot, regardless of maturity (Sabatino, & Smith, 2008).

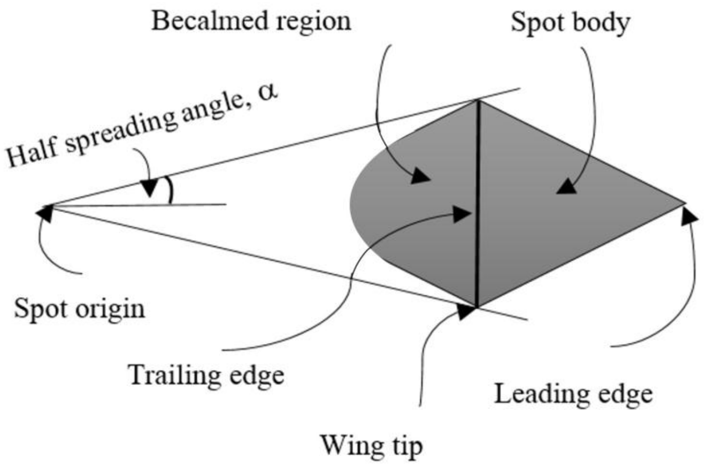

Figure 1 Schematic drawing of a turbulent spot

Makita and Nishizawa (2001) studied a merging process of a pair of turbulent spots using the multi-hotwire system. They discovered that when two turbulent spots merge, the interaction between the longitudinal wingtip vortices gives birth to a strong upwash in the merged region. This strong upwash induces an inflectional velocity profile and then enhanced spanwise vortices at the top of the merged spot. Krishnan and Sandham (2006) used Direct Numerical Simulation (DNS) to verify the mechanism of longitudinal merging and discovered that calmed region behind the tail of the downstream spot is found to suppress the growth of the upstream spot. The upstream spot was ultimately engulfed by the downstream spot and by a longitudinal merging effect may be responsible, rather than the decay in the perturbation energy (Casper et al., 2012).

1.2. Thermochromic liquid crystal

In 1888, Reinitzer (1888) carried out the experiment on the cholesteryl benzoate and first discovered the birefringence properties of liquid crystals. Thermochromic liquid crystals - TLCs have been widely used by researchers in heat transfer and fluid flow communities as a thermal imaging tool to show surface and spatial temperature distributions. They are essentially characterized by a helical molecular structure, stretching as a function of temperature. When illuminated with white light, the liquid crystals selectively reflect monochromatic light with a wavelength that equals to the pitch of the helical structure. When their temperature is increasing, the wavelength of the reflecting light changes from red to blue through the visible spectrum. The initial calibration process is necessary to define the color–temperature relationship of the liquid crystals in order to apply them for the quantitative temperature measurements. Abdullah et al. (2010) provided useful information to novice and intermediate users for the calibration process of the liquid crystals, particularly for surface thermography. Furthermore, Wiberg and Lior (2004) reported that the important factors affected the precision of liquid crystals were hysteresis, aging, surrounding illumination disturbance, viewing angle, amount of light into the camera, and coating thickness.

Thus, this research investigates the thermal behavior of the flat heating plate underneath the turbulent spots, artificially initiated by two pulsating water jets with a duration of 1 s apart. The jets are injected in an upward direction, perpendicular to the mainstream flow to disturb the laminar boundary layer and cause the longitudinal (tandem) merging process of the spots. In this paper, the flow visualization technique using thermochromic liquid crystals (TLCs) are well explained and used to measure the unsteady surface temperature. With the aid of image processing technique and energy balance, the time-dependent Nusselt number and turbulent spot effectiveness are determined. Also, the thermal characteristics between the tandem merging spots and the single turbulent spot in 2 cases of different water and surface temperature are compared and discussed.

2. Objectives

1. To establish the technique of heat transfer enhancement using the single spot and longitudinal merging spots, which induced by a water injection over a heating plate and also study the thermal characteristic of them.
2. To apply the TLCs in the application of unsteady heat transfer measurement.

3. Materials and Methods

3.1 Experimental setup

This experiment was conducted in a rectangular water flow channel which had a 0.15 m width, a 0.2 m height and a 1 m long as shown in figure 2. Moreover, the mainstream flow is from left to right, so it means the left side of figure 2 is upstream and the right side is downstream. The water flow channel was made from acrylic of 1 cm thick in order to obtain a good view and provide the resistance for the heat loss. The bleeding channel was installed at the inlet of the test plate to bleed the water out and refresh a new boundary layer on the test surface made by an aluminum plate. This surface was covered by a black polyvinyl chloride (PVC) sheet of 0.12 mm thick. The thermochromic liquid crystals (TLCs) were coated on the PVC sheet to measure the temperature distribution of the test plate. They are overcoated by a layer of varnish in order to prevent direct contact between the TLCs and water flow, which can deteriorate the birefringence properties of liquid crystals. In this study, the active range of the TLCs is from 26 ˚C to 30 ˚C, so the experiment was conducted during this temperature range. Three type-K thin leaf thermocouples, having an uncertainty of 0.75 % are well glued on top of the test plate at the streamwise position of 0.364, 0.469 and 0.626 m from the plate leading edge. The temperature, measured by these thermocouples was directly sent to the data logger and correlated with the color of the liquid crystals.

In order to perform an isothermal surface, six commercially plate heaters with the different size were installed under the aluminum plate. They were also controlled by using proportional integral derivative controllers (PID) and dimmers. Hence, the constant temperature surface (T_s) condition can be obtained in 2 cases, i.e. case A has T_s of 28 °C with water temperature (T_w) of 24 °C and case B has T_s of 27 °C with a water temperature of 23 °C through the experiment. In the meantime, the mainstream flow at 0.18 m/s was supplied by a 2.5 HP centrifugal pump. This velocity corresponds to the local Reynolds number of the test region during 61,000 – 130,000. The turbulent spot was created by injected the water through a 1 mm diameter hole in the perpendicular direction of the mainstream flow to disturb the boundary layer at 0.3 m from the plate leading edge. At this position, the boundary layer profile and thickness were measured using a hot film sensor as depicted in figure 3 for 2 cases. The results show that the yielded data agree well the Blasius profile and the laminar boundary layer thickness is δ_0 = 0.006 m, referring to the boundary layer displacement thickness, δ^* of 0.002 m. The turbulence intensity of the freestream flow is 1.12 %.

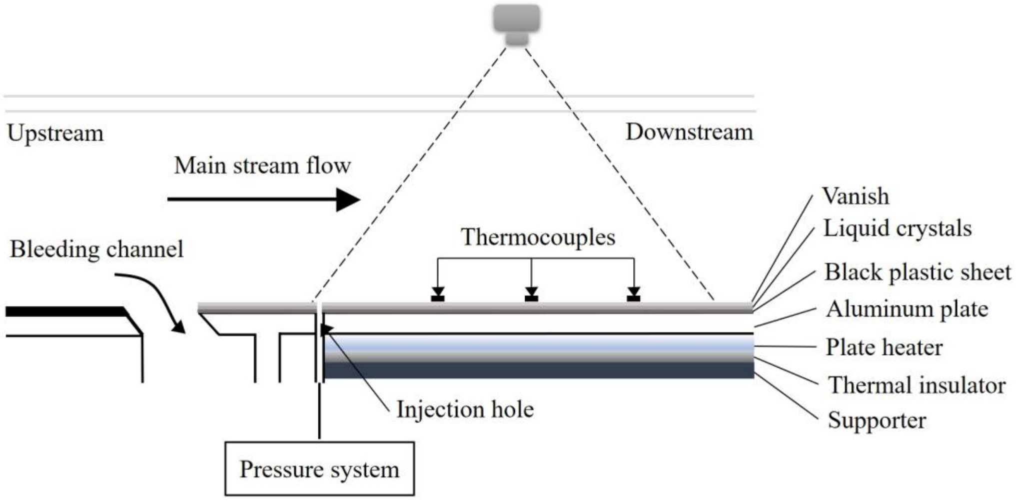

Figure 2 Schematic diagram of the test section in the water tunnel

The injector is directly connected with the pressure system as shown in figure 4. The water in this system was fed from the water tank, and its pressure was controlled by a diaphragm tank, mounted with the air pump to keep the pressure at 3 bars through the test. Afterward, each trigger was done manually with the help of the programmable logic controller (PLC) system via a solenoid valve. Thus, the injection was kept at the different velocities of 13 m/s in case A and 15 m/s in case B, respectively, as shown in table 1.

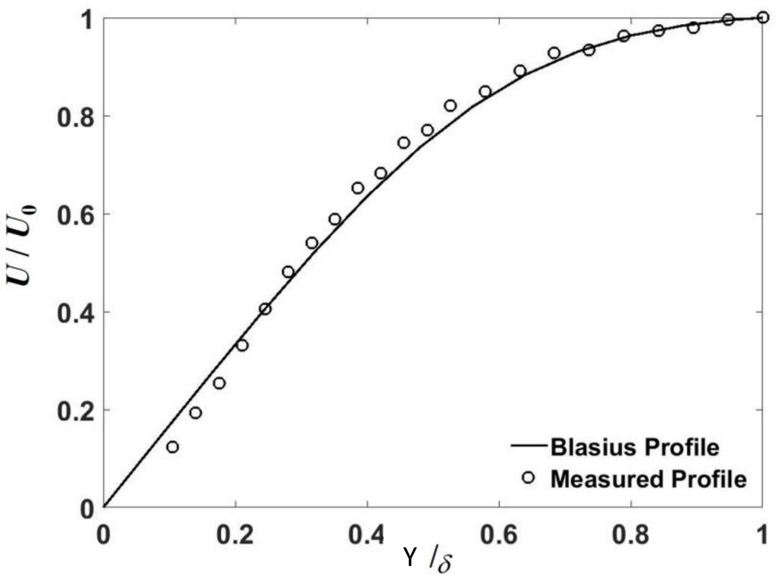

Figure 3 Measured boundary layer profile at the location of spot generator, where U is the measured velocity (m/s); U_0 is the free stream velocity (m/s); Y is the height of measuring position (m); δ is the laminar boundary layer thickness (m).

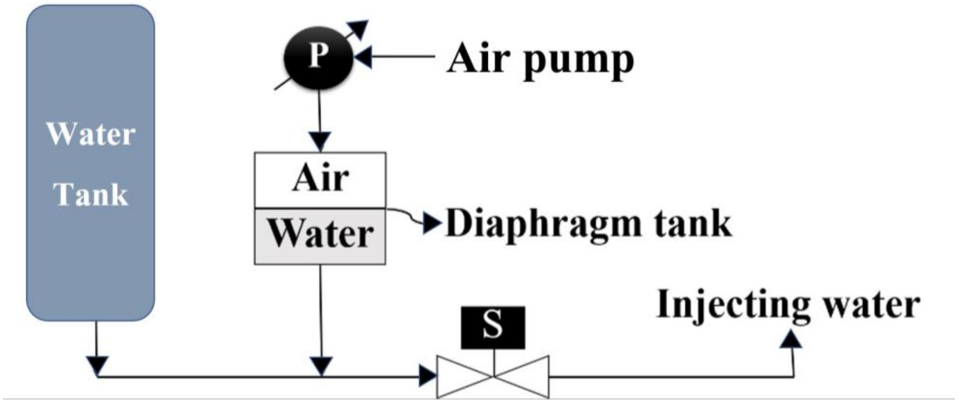

Figure 4 Pressure system of the spot generator

Table 1 The different condition of the experiment

	Case A	Case B	Unit
T_s	28	27	°C
T_0	24	23	°C
Injected velocity (V_{inj})	13	15	m/s

Two fluorescent bulbs having a diameter of 2.5 cm was installed beside the test section to illuminate the white light on the coating TLCs. Their light intensity was strengthened by a glossy reflector, mounted with each bulb. A video camera was installed at 1.5 m above the test surface to record the color change of liquid crystals with a frame rate of 25 fps.

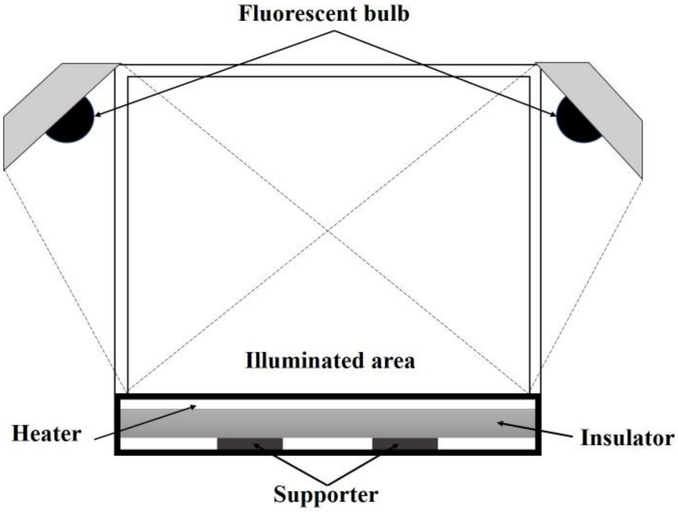

Figure 5 Side view of the test section

3.2. Mathematical analysis

Before use, the color of thermochromic liquid crystals must be correlated via a calibration process with the method following Chaiworapuek and Kittichaikarn (2016). In the experiment, the video camera firstly collected the images in RGB system, comprising Red, Green, and Blue signals. For the convenience of the calculation, this system was changed to HSI system or Hue, Intensity, and Saturation signals. The relation between Hue and RGB system is given by Russ (2002) as:

$$H = cos^{-1}(Z) \quad \text{if} \quad G \geq R \tag{1}$$

$$H = 2\pi - cos^{-1}(Z) \quad \text{if} \quad G < R \tag{2}$$

$$Z= (2B-G-R)/(2*[(B-G)^2+(B-R)/(G-R)]^{1/2}) \tag{3}$$

Where H = Hue signal value
R = Red signal value
G = Green signal value
B = Blue signal value

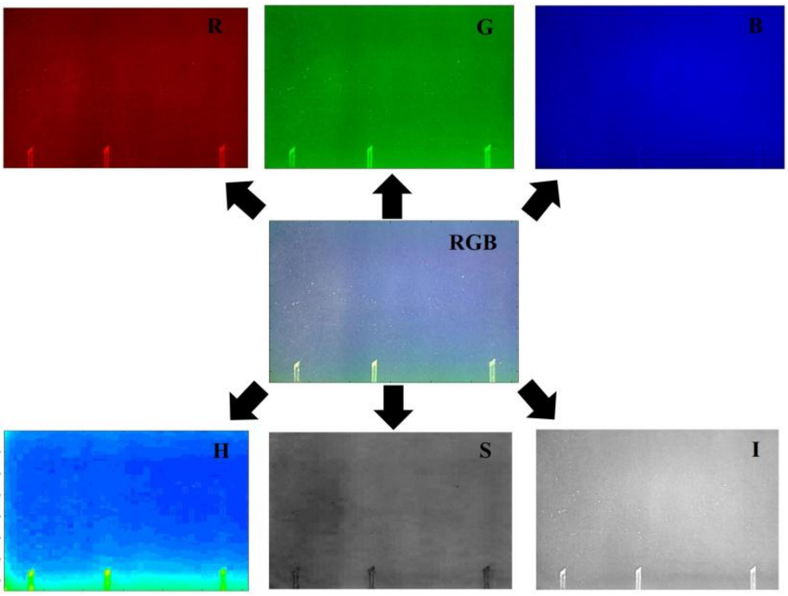

Figure 6 Various signals in the RGB system and HSI system

In figure 6 show the Various signals in the RGB system and HSI system from the experiment. The relation between Hue and surface temperature in the calibration process must be obtained at the same condition as the turbulent spot test. Each color of liquid crystals at a thermocouple is recorded through the temperature from 25.6 °C to 27.4 °C with an increment of 0.2 °C. The relation between the color of liquid crystals and surface temperature was fit by a fifth order polynomial equation as shown in figure 7. This equation has the R^2 of 0.9982 and is given as:

$$T = 1495.1H^5 – 3220.8H^4 +2728H^3– 1128.8H^2 + 230.38H+ 7.1018 \tag{4}$$

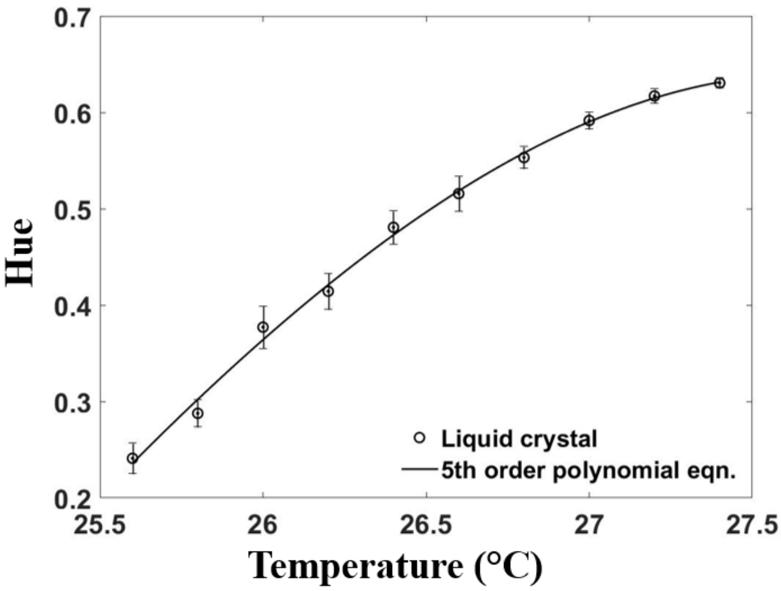

Figure 7 Calibrated relation between hue and temperature

The local Reynolds number on the flat plate can be determined as:

$$Re_x = \rho U_0 x / \mu \tag{5}$$

Where ρ = density of water (kg/m^3)
U_0 = freestream velocity (m/s)
x = streamwise distance from the plate leading edge (m)
μ = dynamic viscosity of water (kg/m·s)

Following Kays et al. (2005) the local Nusselt numbers for laminar flow and heat transfer coefficient can be determined as:

$$Nu_x = [0.332 Re_x^{1/2}\, Pr^{1/3}] / [1 - (\xi / x)^{3/4}]^{1/3} \tag{6}$$

Where Pr = Prandtl number
ξ = unheated starting length (m)

The obtained heat flux is explained from Newton's law of cooling, so can be determined as:

$$q_x = h_x(T_s - T_0) \tag{7}$$

and Nusselt numbers determined as

$$Nu_x = h_x x / k \tag{8}$$

Where q_x = heat flux (W/m^2)
h_x = local heat transfer coefficient (W/m^2·˚C)
T_s = surface temperature (˚C)
T_0 = freestream temperature (˚C)
k = thermal conductivity (W/m·˚C)

The local Nusselt number on the heating surface without the turbulent spot obtained in this study was validated with those from the correlation of Kays et al. (2005) as depicted in figure 6. The comparison shows that they are consistent during the local Reynolds number between 61,000 and 130,000. This confirms the reliability of the experimental set up of the current study.

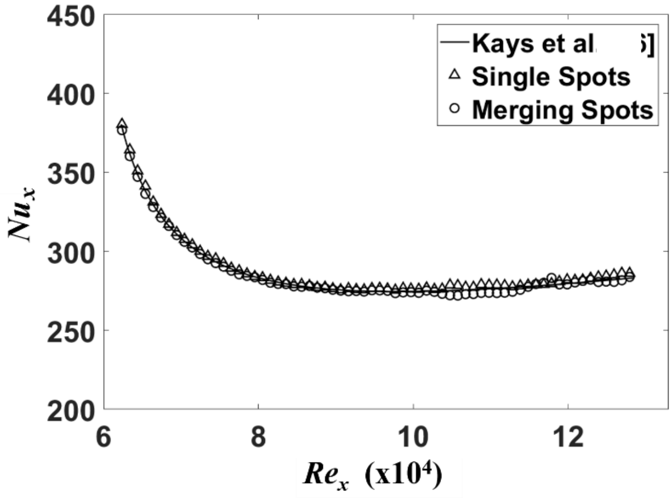

Figure 8 Comparison of the local Nusselt number from the experiment and the results calculated by the correlation of Kays et al. (2005)

The dimensionless of time τ is used to define the floating time after the spot initiation. It can be determined as:

$$\tau = t / (\delta^* / U_0) \tag{9}$$

Where t = time (s)
δ^* = boundary layer displacement thickness at the water injection (m)

In the present experiment, the second turbulent spot was generated after the first spot 0.5 and 1 second, corresponding to the $\Delta\tau$ of 50.53 and 101.76, respectively.

4. Results and Discussion

Thermal structure of the turbulent spot footprint was induced by the water injection. The results from the video were conversed to picture as RGB system. The spot evolution under these conditions is presented in the form of the normalized temperature contour as the example by case B in Figure 9 which evaluated as follows:

$$\theta = (T - T_0) / (T_s - T_0) \tag{10}$$

At τ = 0 or the time before the turbulent spot arrival, the temperature of the test surface (T_s) was kept at 28.0 °C in case A with freestream temperature or water temperature (T_0) of 24.0 °C and 27.0 °C with T_0 of 23.0 °C in case B. For heating flat without turbulent spot was calculated via Equation (10) for each case. Hence, it demonstrated the normalized temperature contour by θ = 1. Noted that the θ in the region of thermocouples is also set as 1 to avoid the error during the calculation. The θ contours under case A and B have a common freestream velocity of 0.18 m/s, so the Re_x presenting the streamwise distance is set to 61,000 - 130,000. Meanwhile, the dimensionless spanwise distance is displayed between -45 and 45 and the images were captured at τ = 202.12 for single spot ($\Delta\tau$ = 0) and longitudinal merging spots ($\Delta\tau$ = 50.53 and

101.76). For example, in case B, the disturbance occurring over the heating surface appeared had four streaks, consequent from the merging hairpin vortices in the upper layer flow. The structure of disturbance enlarges in both streamwise and spanwise directions and also more streaks occur as the structure propagates downstream.

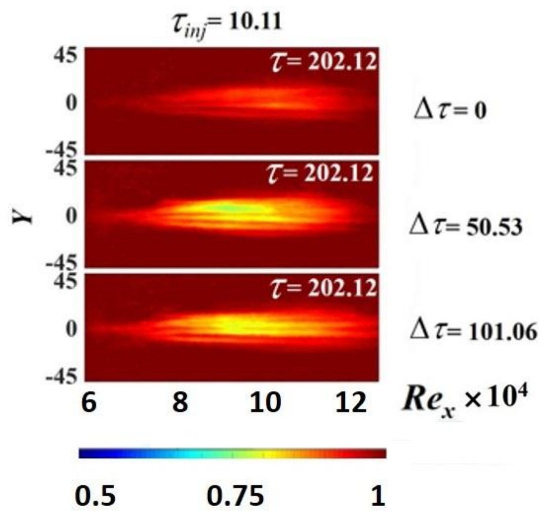

Figure 9 The contour of temperature of single spot ($\Delta\tau$ = 0) and longitudinal merging spots ($\Delta\tau$ = 50.53 and 101.76) from case B (v_{inj} = 15 m/s)

Besides, the images of the test region were recorded in RGB format. They were converted to Hue signal and the surface temperature via Equation 1 – 3 and Equation 4, respectively. Figure 10 presents the contour of *Nu* of single spot and longitudinal merging spots in for case B. The magnitude of Nu was between 200 – 500, which labeled in the below the color bar. The x-axis refers to the Re_x between 61,000 – 130,000 while the dimensionless spanwise distance, $Y = y / \delta^*$, was between -45 and 45. At each τ, the upper and the lower windows depicted the *Nu* of the single turbulent spot and longitudinal merging spots, respectively. The figure shows that the turbulent spots were initiated by the water injection and have the streaky structure similar to those yielded by Rakpakdee and Chaiworapuek (2016). The spots enhanced the heat transfer of the heating surface, and the maximum Nusselt number appears at their centers. It was increasing when it convected further downstream. The maximum *Nu* of the longitudinal merging spots is 580.7 with $\Delta\tau$ = 101.76.

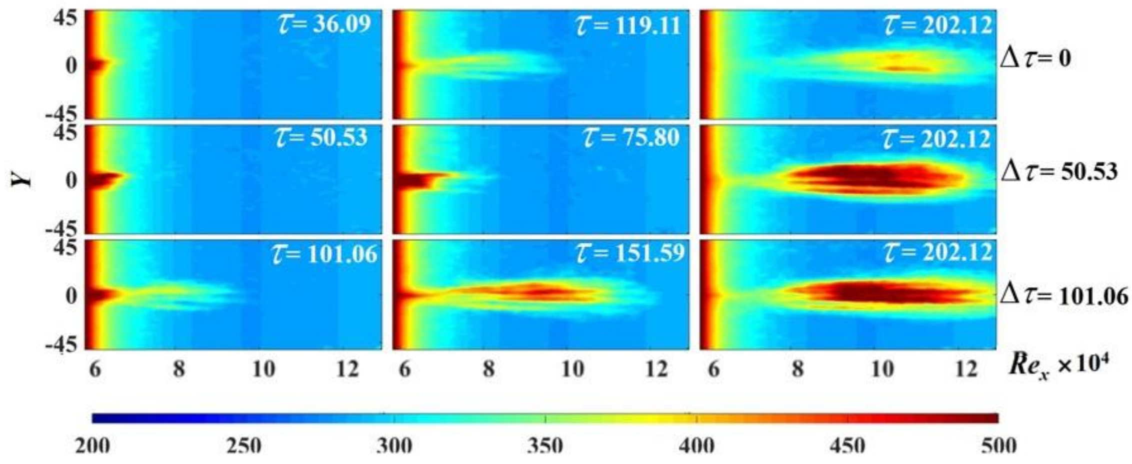

Figure 10 The contour of *Nu* of single spot and longitudinal merging spots from case B

The contours of the turbulent spot effectiveness, $Q_{ef} = q_s / q_{ns}$ are presented at each τ, the upper and the lower windows depict the Q_{ef} of the single turbulent spot and longitudinal merging spots, respectively. The q_s and q_{ns} are the heat flux in the spot bound under the condition with and without turbulent spot, respectively. Its magnitude of 1 – 1.45 can be deduced from the below color bar. Typically, the heat transfer area in Q_{ef} contours can represent by the spot structure where the characteristic of the Q_{ef} is similar to the ration of the Nusselt number. However, the percentage that increased above the laminar level is different from the *Nu* distribution. In Figure 11, the maximum Q_{ef} of the longitudinal merging spots is more than 1.58 and also more than the value achieved from a single spot. As suggestions of (Cantwell et al., 1978; Sabatino, & Smih, 2008; Johnson, 1999) the turbulent spot accumulates the warmer fluid into the upper structure from which region it passes like a sweeping process. Thus, the area behind the structure is then replaced by the colder water from the upper layer, and this causes a reduction in temperature via a turbulent spot on a heating plate.

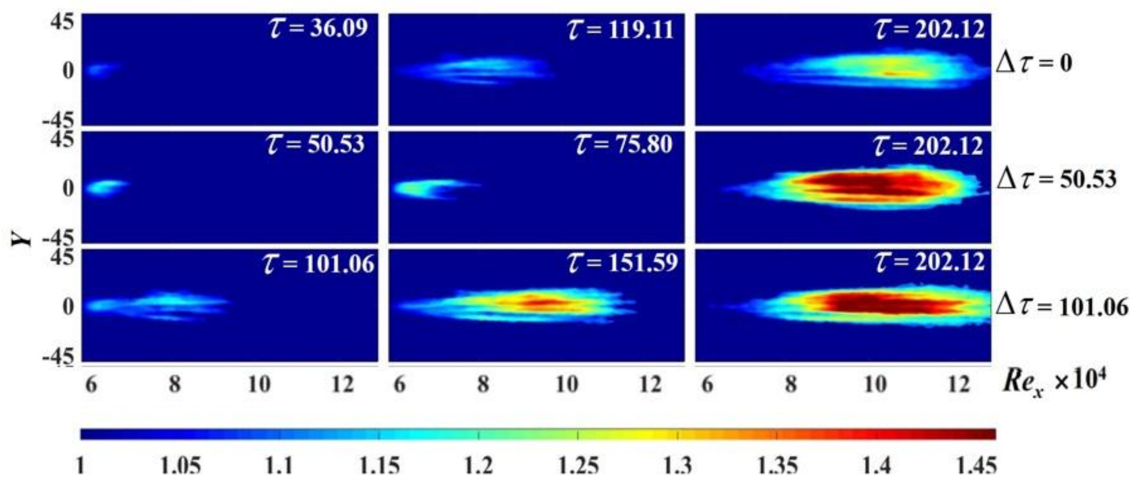

Figure 11 The contour of Q_{ef} of single spot and longitudinal merging spots from case B

In this study, the *Nu* was obtained under the freestream velocity of 0.18 m/s of case A and B. During τ = 25 to 200; it is found that highest *Nu* occurs during τ = 25 to 50. This characteristic, presenting behavior of young turbulent spot was in agreement with the results, provided by Chaiworapuek and Kittichaikarn (2016). The procreation of turbulent spot, after the jet strength weakened, this accumulated energy was released forward in downward direction and impact on the heating surface. This process forms a primary hairpin vortex, leading to the regeneration of other hairpin vortices to organize a turbulent spot. Also, it brings the colder water from the upper layer directly to the hot surface and high heat exchange at the moment after the injection. So, by longer injecting duration obtains a higher Nu because of the previous behavior. Moreover, this also generates a higher local pressure and creates a higher impact on the heating surface when the blocked water gushes forward in the downward direction. This directly causes a higher maximum Nu and average Nu of the turbulent spot. The average Nusselt number increases again following its maturity. Before the second spot is induced, the characteristic and the value of Nu_{avg} are similar. However, another injection provides the second increase before the minimum Nu_{avg}, but it is noted that this is less than the maximum Nu_{avg} from the first injection. Figure 12 shows that these 2 cases of single spot have the same results to have the same different temperature at 4 °C between water temperature and surface temperature. From this reason longitudinal merging spots between case A and B were comparable.

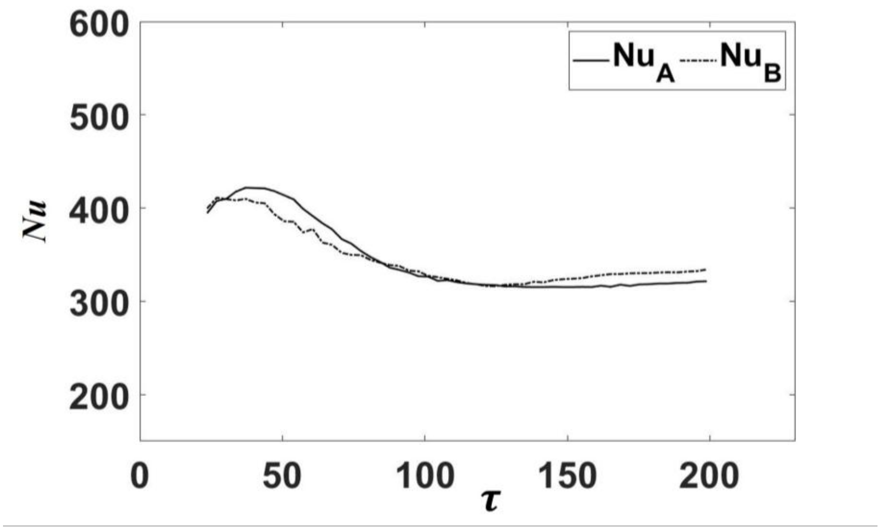

Figure 12 The comparison of *Nu* of single spot between case A and case B

In Figure 13 show *Nu* of the single spot of case A and B. At τ = 202.28, the maximum magnitude of *Nu* occurs at the core of the structure. For both case when the single spot (Nu_A and Nu_B) is compared with longitudinal merging spots (Nu_{A1}, Nu_{B1}), they behave similarly at τ from 25 – 50.53 because the second spot has not been initiated yet. The highest *Nu* occur in longitudinal merging spots by both cases which is 418.80 and 439.23 in case A (Nu_{A1}) and case B (Nu_{B1}), respectively. At τ = 50.53, the second pulse has been already injected to create the second turbulent spot. This creation results in the higher *Nu* at the upstream region comparing with the single spot at τ = 202.28. The average *Nu* inside the turbulent spot bound is plotted against the τ as shown in figure 14. The results of the single spot are in agreement with those yielded from Chaiworapuek and Kittichaikarn (2016). The first maximum *Nu* is from the effect of the water injection due to its maturity. Meanwhile, the characteristic of the Nusselt number ratio is consistent with the result of the single spot. After the second pulse is injected at τ = 50.53, the magnitude of *Nu* increases again and it is relatively higher than those obtained from the single turbulent spot when the spots fully unite at τ = 202.28, at this point, the single spot and longitudinal merging spots for each case were compared, and the results show the *Nu* of longitudinal merging spots were more than the single spot in case A it increased 1.5 % and increased 20 % in case B.

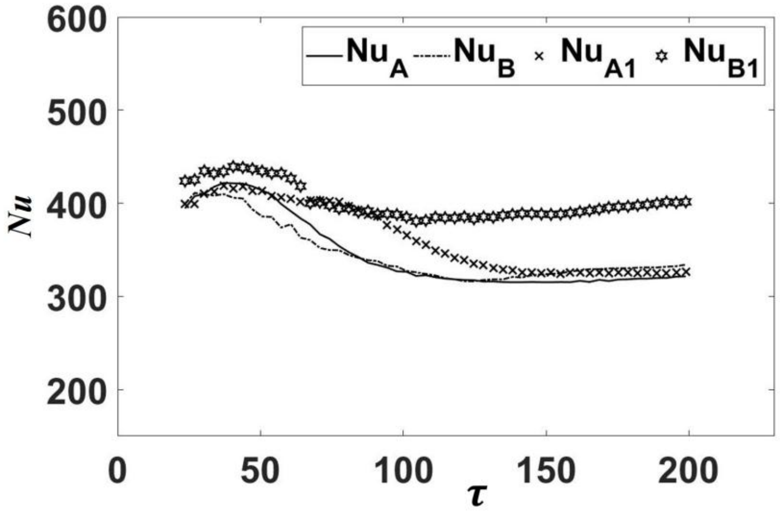

Figure 13 The comparison of *Nu* of single spot and longitudinal merging spots between case A and case B with $\Delta\tau = 50.53$

Figure 14 shows *Nu* of the single spot of case A and B. At $\tau = 202.28$, the maximum magnitude of *Nu* occurs at the core of the structure. For both case when the single spot (Nu_A and Nu_B) is compared with longitudinal merging spots (Nu_{A2} and Nu_{B2}), they behave similarly at τ from 25 - 84.28 because the second spot has not been initiated yet. The highest *Nu* occur in longitudinal merging spots by both cases which is 430.07 and 438.17 in case A (Nu_{A2}) and case B (Nu_{B2}), respectively. At $\tau = 101.06$, the second pulse has been already injected to create the second turbulent spot. This creation results in the higher *Nu* at the upstream region comparing with the single spot at $\tau = 202.28$. The average *Nu* inside the turbulent spot bound is plotted against the τ as shown in figure 14. The first maximum around 430 of all case is from the effect of the water injection due to its maturity. Meanwhile, the characteristic of the Nusselt number ratio is consistent with the result of the single spot. After the second pulse is injected at $\tau = 101.06$, the magnitude of *Nu* increases again, and it is relatively higher than those obtained from the single turbulent spot. when the spots fully unite at $\tau = 202.28$, at this point, the single spot and longitudinal merging spots for each case were compared, and the results show the *Nu* of longitudinal merging spots were more than the single spot in case A increased 8 % and increased 20 % in case B.

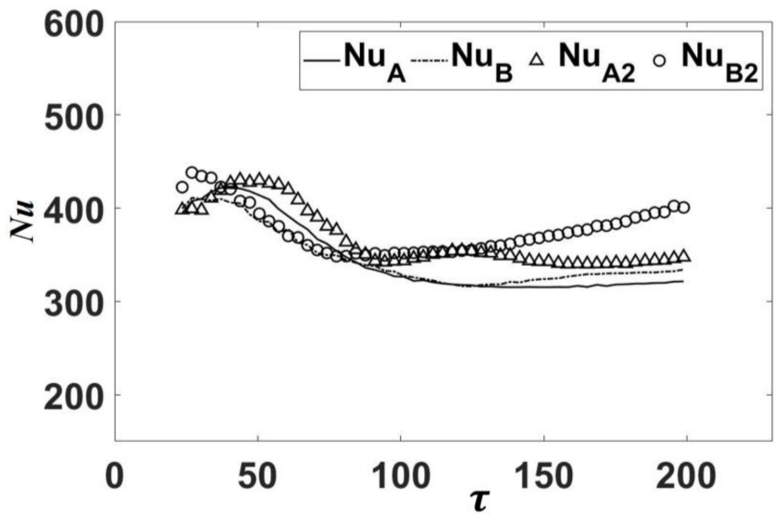

Figure 14 The comparison of *Nu* of single spot and longitudinal merging spots between case A and case B with $\Delta\tau = 101.06$

Figure 15 illustrates the characteristic of the average Q_{ef}, determined inside the spot bound during $\tau = 0 - 200$. The comparison of Q_{ef} of single spot and longitudinal merging spots against τ clearly shows that the longitudinal merging spots provide more Q_{ef} than those yielded from single spot since $\tau = 50.53$., So at 202.28 obtain the results that in case A, it is 1.12 or increasing only 0.3 % of its single spot and in case B, it is 1.29 or increasing 11.92 % of its single spot. After the Q_{ef} of single spot reaches the minimum value after the first peak, the magnitude increases again by the effect of the spot maturity.

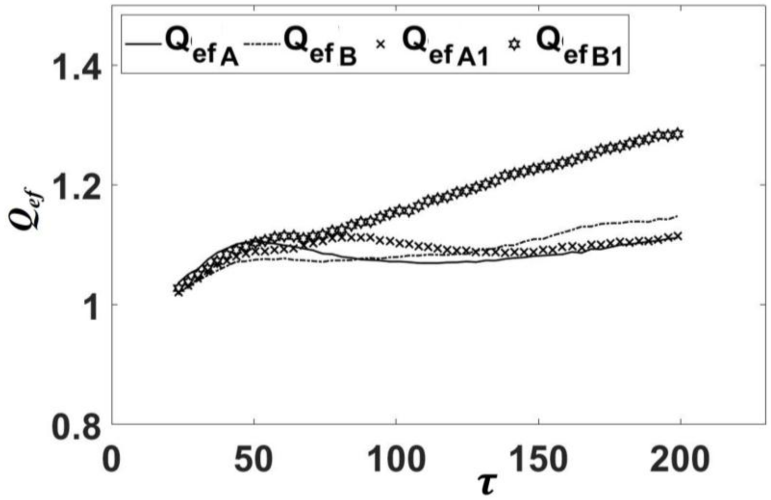

Figure 15 The comparison of Q_{ef} of single spot and longitudinal merging spots between case A and case B with $\Delta\tau = 50.53$

Figure 16 illustrates the characteristic of the average Q_{ef}, determined inside the spot bound during τ = 0 – 200. The comparison of Q_{ef} of single spot and longitudinal merging spots against τ clearly shows that the longitudinal merging spots provide more Q_{ef} than those yielded from single spot since τ = 101.06., So at 202.28 obtain the results that in case A, it is 1.19 or increasing only 6.3 % of its single spot and in case B, it is 1.28 or increasing 11.9 % of its single spot. After the Q_{ef} of single spot reaches the minimum value after the first peak, the magnitude increases again by the effect of the spot maturity.

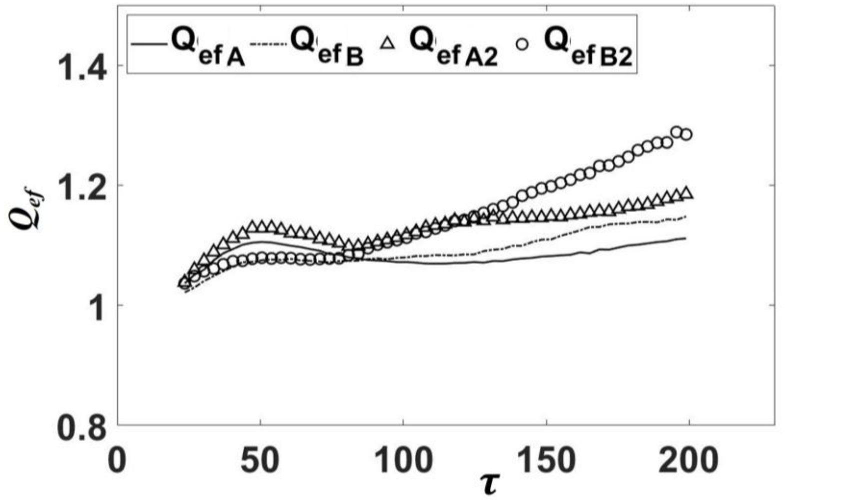

Figure 16 The comparison of Q_{ef} of single spot and longitudinal merging spots between case A and case B with $\Delta\tau$ = 101.06

5. Conclusion

By using thermochromic liquid crystals, this study presents the behavior of heat transfer enhancement via the longitudinal merging spots induced by the small pulsating jet in the perpendicular direction of the mainstream. The experiment was carried out over the local Reynolds number between 61,000 and 130,000. It was tested single spot and longitudinal merging spots which were formed by the different duration of water injection which was 50.53 and 101.06 s. It is divided in 2 cases with the difference of isothermal surface, the temperature of the mainstream and injected velocity, i.e. case A having 28 °C, 24 °C and 13 m/s, respectively and Case B having 27 °C, 23 °C and 15 m/s, respectively. The results of single spot have nearly the same because there is a similar difference range at 4 °C. The results of single spot and longitudinal merging spots show that the *Nu* and Q_{ef} of longitudinal merging spots are more than those yielded from single spot around 1.5-20 % and 0.3-11.92 %, respectively because it was found that the growth of 2nd spot was highly suppressed becalmed region of a 1st spot (Krishnan, & Sandham, 2006). Meanwhile, in his research, the results of longitudinal merging spots show that more injected velocity has more *Nu* and Q_{ef} i.e. 18.5 % and 6 %, respectively. Thus, the inline injecting duration, accumulating more local pressure directly causes a bigger impact on the flat plate. Consequently, the magnitude of Nusselt number and effectiveness of mature turbulent spot are proportional to injecting time (Rakpakdee et al., 2019), so in this research when more v_{inj} are required, it has to use more time to inject.

6. Acknowledgments

The authors would like to acknowledge the financial support from the Thailand Research Fund (TRF) - MRG5980056 and gratefully thank Asst. Prof. Dr. Weerachai Chaiworapuek for the valuable advice.

7. References

Abdullah, N., Talib, A. R., Abu, Jaafar, A. A., Mohd, Salleh, M. A., Chong, W. T. (2010). The basics and issues of thermochromic liquid crystal calibrations. *Experimental Thermal and Fluid Science*, *34*,1089-1121.

Cantwell, B., Coles, D., Dimotakis, P. (1978). Structure and entrainment in the plane of symmetry of a turbulent spot, *J. Fluid Mech, 87*(4) 641-672.

Casper, K. M., Beresh, S. J., Schneider, S. P. (2012). A Preliminary Study of the Longitudinal Merging of Instability Wave Packets and Turbulent Spots in a Hypersonic Boundary Layer. *American Institute of Aeronautics and Astronautics*, 1-15. Retrieved from https://www.osti.gov/servlets/purl/1117119

Chaiworapuek, W., Kittichaikarn, C. (2016). On the thermal and structural characteristics of an artificially generated young turbulent spot. *International Journal of Heat and Mass Transfer*, *92*, 850–858.

Elder, J. W. (1960). An experimental investigation of turbulent spots and breakdown to turbulence. *Journal of Fluid Mechanics*, *9*(2), 235-246.

Emmons, H. W. (1951). The laminar-turbulent transition in a boundary layer-part I. *Journal of Aerospace Science*, *18*, 490–498.

Johnson, M. W. (1999). Prediction of turbulent spot growth rates. *Proceedings of International Gas Turbine & Aeroengine Congress & Exhibition*, Indianapolis, Indiana, USA, 99-GT-031, V003T01A005.

Kays, W. M., Crawford, M. E., Weigand, B. (2005). *Convective Heat and Mass Transfer* (4th edition). New York: McGraw-Hill.

Krishnan, L., Sandham, N. D. (2006). On the merging of turbulent spots in a supersonic boundary-layer flow. *International Journal of Heat and Fluid Flow, 27*, 542–550.

Makita, H., Nishizawa, A. (2001). Characteristics of internal vortical structures in a merged turbulent spot. *Journal of turbulence*, *2*, 1468-5248.

Rakpakdee, W., Chaiworapuek, W. (2017). Heat Transfer Enhancement in Laminar Flow over Flat Plate Using Small Pulsating Jet. *The 7th TSME International Conference on Mechanical Engineering (Chiang mai: Thailand), 5*(1), 20-29.

Rakpakdee, W., Kittichaikarn, C., Chaiworapuek, W. (2019). Effect of boundary layer destabilization by a water jet on thermal and structural behavior of turbulent spot footprints. *International Journal of Heat and Mass Transfer*, *135*, 491-510.

Reinitzer, F. (1888). Beiträge zur Kenntniss des Cholesterins. *Wiener Monatschr Fur Chem*, *9*, 421-441.

Russ, J. C. (2002). *The image processing handbook* (4th edition). *Materials Science and Engineering Department North Carolina State University Raleigh*, North Carolina, CRC Press Boca Raton London New York Washington, D. C.

Sabatino, D., Smith, C. R. (2008). Turbulent spot flow topology and mechanisms for surface heat transfer. *Journal of Fluid Mechanics*, *612*, 81-105.

Schubauer, G. B., Klebanoff, P. S. (1955). Contribution on the Mechanism of Boundary Layer Transition, *National Advisory Committee for Aeronautics*, *3489*, 31.

Sokolov, M., Antonia, R. A., Chambers, A. J. (1986). A turbulent spot in a two-dimensional duct. *Journal of Fluid Mechanics*, *166*, 211-225.

Wiberg, R., Lior, N. (2004). Error in thermochromic liquid crystal thermometry. *Rev. Sci. Instrum. 75*(9), 2958-2994.

Wu, X., Moin, P. (2010). Transitional and turbulent boundary layer with heat transfer. *Phys. Fluids*, *22*, 085105.

Wygnanski, I., Sokolov, M., Friedman, D. (1976). On a turbulent ‘spot’ in a laminar boundary layer, *Journal of Fluid Mechanics*, *78*(4), 785-819.